Theoretical Design of an Aromatic Hydrocarbon Rotor Driven by a Circularly Polarized Electric Field†

Masahiro Yamaki,‡ Kunihito Hoki,‡ Takato Teranishi,‡ Wilfredo Credo Chung,‡ Fabio Pichierri,§ Hirohiko Kono,‡ and Yuichi Fujimura*,‡

Department of Chemistry, Graduate School of Science, Tohoku University, Sendai 980-8578, Japan, COE Laboratory, Tohoku University, IMRAM, 2-1-1 Katahira, Aoba-ku, Sendai 980-8577, Japan

Received: May 22, 2007; In Final Form: July 8, 2007

An aromatic hydrocarbon rotor without functional groups is theoretically designed. Such a molecular rotor is free from long-range electrostatic interactions. Induced dipole interactions are the rotor-driving forces under a nonresonant excitation condition. As an example, a molecular rotor with a condensed aromatic ring, a pentacene moiety mounted on a phenyl-acetylene axle that is driven by a circularly polarized electric field is considered. Results of simulations of the quantum dynamics of a rotor that take into account short-range rotor−bath interactions are presented by numerically solving the density matrix equations of the rotational motions.

1. Introduction

In recent years, molecular rotors (motors) have been studied from both experimental and theoretical points of view.[1−15] Special attention has been given to optical electric-field-driven molecular rotors.[16−21] It has been shown that rotational motions can be controlled by optimizing variables of optical electric fields such as polarization direction, central frequency, pulse width, and so on.[21] The rotary arm of the rotor consists of a functional group such as NO_2 or CHO, whose dipole moment is of a magnitude that is sufficiently large for the rotor to be driven by electromagnetic fields of reasonably low intensities. On the other hand, such a molecular rotor is subjected to environmental perturbations, especially through long-range electrostatic interactions. This may cause a decrease in rotational power. Therefore, it is worth designing a molecular rotor without any functional group that is free from long-range electrostatic interactions. One of the candidates is a rotor made of hydrocarbon compounds without functional groups that consists of anisotropic, condensed aromatic rings that have a high polarizability to be driven by electromagnetic fields.

In this paper, we first present results of a theoretical design of an aromatic hydrocarbon rotor driven by a circularly polarized electromagnetic field. The rotor designed consists of a rotational arm, a shaft, and a base, which are made of pure hydrocarbons with a condensed aromatic ring. Similar aromatic hydrocarbons have actually been synthesized for molecular rotors.[22−23] We next present results of quantum dynamics simulation of the rotor by evaluating time-dependent expectation values of the rotational angular momentum operator. We clarify dephasing effects on the rotator dynamics by using the Redfield equation with secular approximation. Short-range collisions between the rotor and atoms or molecules in the environment are the main cause of rotational power loss of rotors.

† Part of the "Sheng Hsien Lin Festschrift".

* Corresponding author. E-mail: fujimurayuichi@mail.tains.tohoku.ac.jp. Telephone: +81 22 795 7715. Fax: +81 22 795 7715.

‡ Department of Chemistry, Graduate School of Science, Tohoku University.

§ COE Laboratory, Tohoku University.

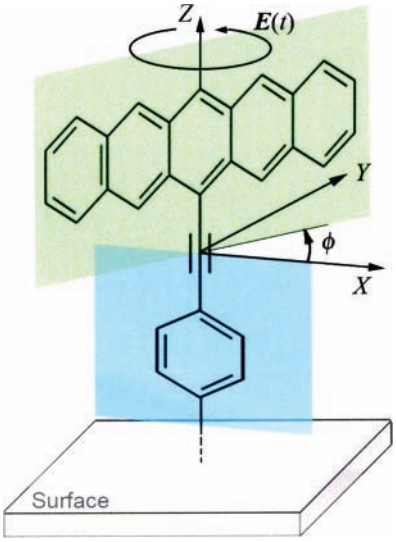

Figure 1. Molecular rotor that has pentacene as its engine attached to a surface through an acetylene unit and a benzene ring. Its rotation is induced by a circularly polarized electromagnetic field.

In the next section, we first describe the time-dependent interaction Hamiltonian in the Born−Oppenheimer approximation within the semiclassical treatment of the rotor−radiation field interaction. We then show an outline of rotor dynamics in the density matrix formalism based on the so-called Redfield theory to take into account short-range interactions between a rotor and atoms or molecules in the heat bath. In Section 3, we present results of quantum dynamic simulations of a real molecular rotor, pentacene, that is surrounded by colliding substances under finite temperature conditions.

2. Theory

(a) An Aromatic Hydrocarbon Rotor Driven by a Circularly Polarized Time-Dependent Electric Field. Consider an aromatic hydrocarbon rotor attached at a surface as shown in Figure 1. The internal, hindered-rotational coordinate is denoted by ϕ. We restrict ourselves to a one-dimensional rotor, neglect-

10.1021/jp073953t CCC: $37.00
Published on Web 08/24/2007

ing other degrees of freedom of the internal nuclear motions. A circularly polarized electric field of electromagnetic radiation, $\boldsymbol{E}(t)$, with a propagation vector to the Z direction is applied to the molecular rotor. The interaction between the rotor and electric field is treated within the semiclassical treatment. Let the rotor be perturbed by atoms or molecules as a heat bath. Interactions between the electric field and the heat bath are omitted. The total Hamiltonian can be expressed under a nonresonant excitation condition as

$$H(t) = H_S(t) + H_B + H_{SB} \tag{1}$$

where system Hamiltonian $H_S(t)$ describes rotor dynamics in the presence of the electric field $\boldsymbol{E}(t)$, H_B denotes the bath Hamiltonian depending on the other degrees of freedom of the rotor system and the environment, and H_{SB} describes rotor−bath couplings.

The Hamiltonian $H_S(t)$ of the rotor in the electronic ground state is expressed in the Born−Oppenheimer approximation as[25]

$$H_S(t) = -\frac{\hbar^2}{2I}\frac{d^2}{d\phi^2} + U(\phi) - \mu(\phi)\cdot\mathbf{E}(t) - \frac{1}{2}\boldsymbol{E}^{\mathrm{T}}(t)\cdot\alpha(\phi)\cdot\boldsymbol{E}(t) \tag{2}$$

where $U(\phi)$ is the potential energy and I is the moment of inertia of the rotor. We restrict ourselves to the first- and second-order rotor−radiation field interactions and neglect the higher-order interactions $O(E^3)$. The third term in the right-hand side of eq 2 denotes the dipole interaction with dipole moment $\mu(\phi)$, and the fourth term denotes the induced-dipole interaction and $\alpha(\phi)$ is a symmetric polarizability tensor of the rotor. By assuming that the rotor is rigid, the two-dimensional polarizability components of the arm are expressed in terms of sinusoidal functions as

$$\begin{aligned}\alpha(\phi) &\equiv \begin{pmatrix}\alpha_{XX}(\phi) & \alpha_{XY}(\phi)\\ \alpha_{YX}(\phi) & \alpha_{YY}(\phi)\end{pmatrix}\\ &= \begin{pmatrix}\cos(\phi) & -\sin(\phi)\\ \sin(\phi) & \cos(\phi)\end{pmatrix}\begin{pmatrix}\alpha_{XX}(0) & 0\\ 0 & a_{YY}(0)\end{pmatrix}\begin{pmatrix}\cos(\phi) & \sin(\phi)\\ -\sin(\phi) & \cos(\phi)\end{pmatrix}\\ &= A\begin{pmatrix}1 & 0\\ 0 & 1\end{pmatrix} + B\begin{pmatrix}\cos(2\phi) & \sin(2\phi)\\ \sin(2\phi) & -\cos(2\phi)\end{pmatrix}\end{aligned} \tag{3}$$

Here, the first term expresses the isotropic components of the polarizability and $A = \{\alpha_{XX}(0) + \alpha_{YY}(0)\}/2$, and the second term the anisotropic components and $B = \{\alpha_{XX}(\phi) - \alpha_{YY}(\phi)\}/2$.

Let $\boldsymbol{E}^{\pm}(t)$, a circularly polarized electric field with an envelope of a sine square, be given by

$$\mathbf{E}^{\pm}(t) \equiv \begin{pmatrix}E_X^{\pm}(t)\\ E_Y^{\pm}(t)\end{pmatrix} = \frac{E_0}{\sqrt{2}}\sin^2\left(\frac{\pi t}{\tau_p}\right)\begin{pmatrix}\cos(\omega_p t)\\ \pm\sin(\omega_p t)\end{pmatrix} \tag{4}$$

where E_0 is the amplitude, ω_p is the central frequency, and τ_p is the duration of the electric field. The plus (minus) sign in eq 4 donates the right-handed (left-handed) circularly polarized electric field. The fourth term in the right-hand side of eq 2 is then expressed in an analytical form as

$$-\frac{1}{2}\boldsymbol{E}^{\pm\mathrm{T}}(t)\cdot\alpha(\phi)\cdot\mathbf{E}^{\pm}(t) = -\frac{{E_0}^2}{4}\sin^2\left(\frac{\pi t}{\tau_p}\right)[A + B\cos\{2(\phi \mp \omega_p t)\}] \tag{5}$$

The term in the right-hand side involving A of eq 5 is independent of ϕ and contributes to a potential energy shift of the rotor. The term in involving B eq 5 is the time-dependent interaction between an aromatic hydrocarbon rotor and a circularly polarized optical electric field. Because B is the difference between the diagonal elements of the polarizability at $\phi = 0$, a rotor having a largest rotational ability can be designed by choosing aromatic ring molecules with B as large as possible. For example, a pentacene, a linear aromatic polyacene, is the best one among rotors that consist of condensed aromatic ring molecules with five benzene rings. We use the right-handed circularly polarized electric field $\boldsymbol{E}^{+}(t)$ that is simply denoted as $\boldsymbol{E}(t)$ in this paper.

We can roughly estimate the minimum strength of the electric field $E_0^{\min}$ to drive rotations under the condition that the rotor adiabatically follows the continuous circularly polarized electric field. The interaction energy $BE_0^2/2$ that is given in eq 5 leads to

$$E_0^{\min} \sim \sqrt{\frac{2\Delta U}{B}} \tag{6}$$

Here ΔU denotes the internal rotational potential energy barrier.

(b) Quantum Dynamics of a Rotor in a Bath with Short-Range Interactions. We approximately describe the heat bath as an ensemble of harmonic oscillators. The Hamiltonian is given as

$$H_B = \sum_i \hbar\omega_i a_i^{\dagger} a_i \tag{7}$$

where ω_i is frequency, and $a_i^{\dagger}$ and a_i are annihilation and creation operators in the ith harmonic oscillator, respectively. Let the system−bath coupling be given within the lowest order in the displacement of a bath coordinate as

$$H_{SB} = Q(\phi)\sum_i \hbar\kappa_i (a_i^{\dagger} + a_i) \tag{8}$$

Here, $Q(\phi)$ is an operator of the rotor variable ϕ in which both elastic and inelastic interactions between the rotor and heat bath are taken into account. The coupling constant κ_i and spectrum of the bath $J(\omega)$ are chosen in accordance with an Ohmic spectral density as

$$J(\omega) = 2\pi\sum_i {\kappa_i}^2\,\delta(\omega - \omega_i) = \eta\omega\, e^{-\omega/\omega_c} \tag{9}$$

where the strength of the system−bath coupling is determined by the dimensionless parameter η, and the spectral takes the maximum value at $\omega = \omega_c$.

The time evolution of the rotor is obtained by solving the Redfield equation with secular approximation.[26−28] The evolution of the diagonal elements of the system density matrix is given by

$$\frac{\partial}{\partial t}\rho_{ii}(t) = -\frac{i}{\hbar}\boldsymbol{E}(t)^{\mathrm{T}}\cdot\sum_m [\rho_{im}(t)\alpha_{mi} - \alpha_{im}\rho_{mi}(t)]\cdot\boldsymbol{E}(t) + \sum_{j\neq i} w_{ij}\rho_{jj}(t) - \rho_{ii}(t)\sum_{j\neq i} w_{ij} \tag{10}$$

where each index specifies the matrix element represented by the eigenstates of the field-free system, and the transition probability is $w_{ji} = \Gamma^{+}_{ijji} + \Gamma^{-}_{ijji}$. Here, $\Gamma^{-}_{ijkl} = (\Gamma^{+}_{lkji})^{*}$and

$$\Gamma^{+}_{kijl} = \frac{1}{2\pi} Q_{lj} Q_{ik} \int_0^\infty d\tau \int_0^\infty d\omega J(\omega)\{[\bar{n}(\omega) + 1]\, e^{-i(\omega_{ik}+\omega)\tau} + \bar{n}(\omega)\, e^{-i(\omega_{ik}-\omega)\tau}\} \quad (11)$$

where $\bar{n}(\omega) = \{\exp(\hbar\omega/k_B T) - 1\}^{-1}$ is the Bose distribution, k_B is the Boltzmann constant, T is the temperature, and $\hbar\omega_{ji}$ is the energy difference between the jth and ith field-free system states.

The evolution of the off-diagonal elements is described as

$$\frac{\partial}{\partial t}\rho_{ij}(t) = -i\omega_{ij}\rho_{ij}(t) - \gamma_{ij}\rho_{ij}(t) - \frac{i}{\hbar}\boldsymbol{E}(t)^{\mathrm{T}} \cdot \sum_m [\rho_{im}(t)\alpha_{mj} - \alpha_{im}\rho_{mj}(t)] \cdot \boldsymbol{E}(t) \quad (12)$$

with dephasing rate constant γ_{ij} given as $\gamma_{ij} = \sum_k (\Gamma^{+}_{ikki} + \Gamma^{-}_{jkkj}) - \Gamma^{+}_{jjii} - \Gamma^{-}_{jjii}$.

The initial density operator of the system in the thermal equilibrium $\rho(0)$ is given by the Boltzmann distribution as $\rho_{ij}(0) = \delta_{ij} \exp(-\lambda_i/k_B T)/Z$. Here, δ_{ij} is the Kronecker delta, λ_i is the eigenvalue of the ith field-free system state, and $Z = \sum_i \exp(-\lambda_i/k_B T)$ is the distribution function.

The time-dependent expectation value of the rotational angular momentum operator, $\hat{l} = -i\hbar$ <fr>∂<fd>$\partial\phi$<frx>, $l(t)$, which is a measure of the magnitudes of the rotation dynamics, is defined as

$$l(t) = \mathrm{Tr}\, \hat{l}\rho(t) \quad (13)$$

Here, Tr means to take trace over the quantum states of the rotor. The sign of eq 13 denotes the direction of rotation, and the absolute value denotes the magnitude of the angular momentum.

3. Results and Discussion

We take the molecular system shown in Figure 1 as an aromatic hydrocarbon rotor, which could be synthesized in several laboratories.[22−24] The system has a pentacene unit as an arm of a molecular rotor, which is connected to a surface through a scaffolding part (triple bond and benzene ring). For example, a molecule substituted by sulfurs can be attached onto a gold surface. The axis of rotation is set in the Z-direction and is driven by a transparent, circularly polarized electric field. The origin of the rotation is chosen by setting the dihedral angle between pentacene and the benzene ring at $\phi = 0$, which corresponds to the minimum of the potential energy surface.

Figure 2a shows the potential energy of the rotor arm $U(\phi)$ as a function of the internal rotational coordinate ϕ. The potential energy function was calculated by using the standard DFT (B3LYP/6-31+G**) method.[29] The moment of inertia of the arm is $I = 4321$ amu Å^2.

Figure 2b shows the polarizability components $\alpha_{XX}(\phi)$, $\alpha_{YY}(\phi)$, and $\alpha_{XY}(\phi)$ as a function of ϕ. These components were also calculated within the same level of the DFT method described above. It should be noted that dipole moment $\mu(\phi)$ has no contribution to the rotor dynamics because the symmetry of the rotor belongs to the point group of C_2 (or C_{2v} at $\phi = 0$, $\pi/2$, π, $3\pi/2$). The two-dimensional polarizability tensor of the rotor, $\alpha(\phi)$, is the sum of those of the arm and the scaffolding part, where we considered only those of the arm in eq 3 for simplicity. The calculated polarizability components are fitted well in the form of $\cos(2\phi)$ and $\sin(2\phi)$ in eq 3 with parameters $A = 450$ and $B = 250$ in atomic units, where 1 au = 1.6488×10^{-41} C^2 m^2 J^{-1}.

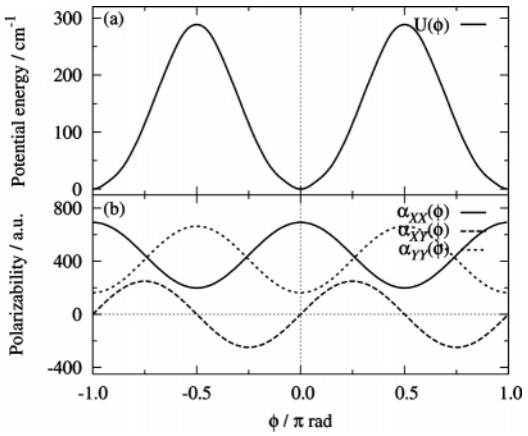

Figure 2. (a) Top panel: the calculated potential energy of the rotor $U(\phi)$ as a function of internal hindered rotational coordinate. (b) Bottom panel: the calculated polarizabilities $\alpha_{XX}(\phi)$, $\alpha_{YY}(\phi)$, and $\alpha_{XY}(\phi)$ of the rotor as a function of ϕ.

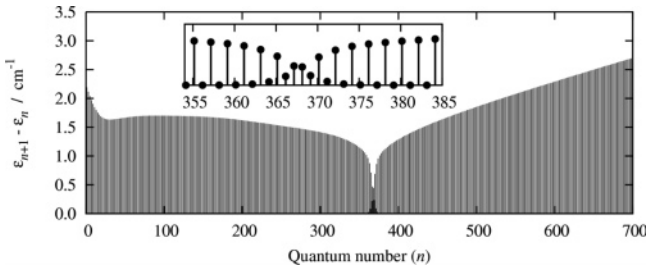

Figure 3. Energy differences in the eigenvalues between the two adjacent eigenstates with quantum numbers $n + 1$ and n. The inserted figure shows an expanded view of the energy around $n = 367$. This is the ordinal energy pattern of a system with a double-well potential.

The eigenvalues $\{\epsilon_n\}$ and eigenvectors of the field-free rotor were obtained by diagonalizing the matrix of H_S with the condition of $\boldsymbol{E}(t) = 0$. Figure 3 shows the differences in the eigenvalues between the two adjacent eigenstates with quantum numbers, $n + 1$ and n. Here, nonzero values in the differences come from $\epsilon_{2k+2} - \epsilon_{2k+1}$, and $\epsilon_{2k+1} - \epsilon_{2k}$ gives almost zero values for $k = 0, 1, 2, \ldots$ within a double-well potential, while such a characteristic feature in the energy differences is reversed in the free-rotational regime (see inserted figure). A dip that appeared around the quantum number $n = 367$ corresponds to the top of the rotational potential energy of $\Delta U = 288$ cm^{-1}. A smooth and flat profile in the eigenvalues can be seen below the dip in Figure 3. A linear dependent behavior above the dip in Figure 3 indicates that the system above the double-well potential can approximately be expressed by a free rotor.

Now consider rotor dynamics in the presence of a right-handed circularly polarized electric field. It should be noted that electric fields are required to prevent field ionizations from the rotor. To choose the appropriate parameters of the electric field, (ω_p, E_0) contour plots of expectation values of the angular momentum at the final time $\tau_p = 0.5$ ns, $l(\tau_p)$ are shown in Figure 4. Here relaxation effects were omitted. There was no significant τ_p dependence in the expectation values. $l(_p)$ for $\tau_p = 0.2-3$ ns. It should be noted that most of the populations were left in the potential well because the electric field used was not optimal one. To rotate the rotor more efficiently, a negative chirp pulse followed by a positive chirp pulse must be applied. This is because the molecular rotor with anharmonic potential has a characteristic structure in both the vibrational and rotational energy level spacing, as shown in Figure 3. A negative chirp pulse can excite the rotor to higher vibrational energy states effectively, and a positive chirp pulse can excite

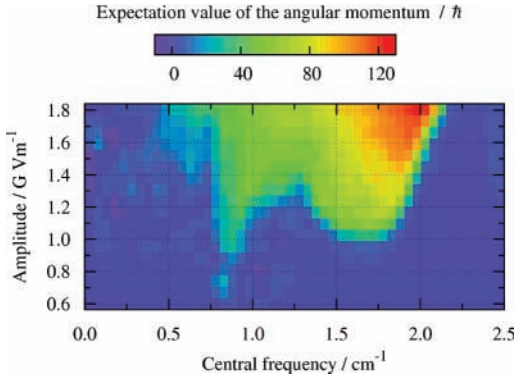

Figure 4. (ω_p, E_0) contour plots of expectation values of the angular momentum at the final time $\tau_p = 0.5$ ns.

the rotor to higher rotational states by a ladder-climbing mechanism.[20e,f] The magnitude of electric field $E_0^{\min}$ suppressing field ionization can be approximated to be that evaluated in the adiabatic following limit, which is estimated to be $E_0^{\min} = 1.7$ GV m^{-1} from eq 6 with parameters $\Delta U = 288$ cm^{-1} and $B = 250$ in atomic units. It can be seen from Figure 4 that there is a broad distribution of ω_p in the range between 0.7−2.1 cm^{-1} for giving an order of tens in $l(\tau_p)$ below the critical electric field of 1.7 GV m^{-1}. The frequency of the minimum value $\omega_p = 0.8$ cm^{-1} is expected to be effective because the induced dipole interaction processes are two-photon processes and the transition frequencies in the potential well are almost 1.6 cm^{-1}, as can be seen in Figure 3. The amplitude of the field E_0 is set to 1.1 GV m^{-1}, which is about $^2/_3$ of the electric field in the adiabatic field limit. This results in a magnitude of 133 cm^{-1} of the rotation-driving field strength $BE_0^2/2$ in eq 5, which is about one half of that of the rotational barrier height, ΔU.

Now we consider the dephasing effects solving the Redfield equations. The frequency ω_c at which the bath spectrum takes the maximum value is set to $\omega_c = 1.4$ cm^{-1}, the temperature in the bath is set to $T = 50$ K, and the periodic function $Q(\phi)$ in eq 7 is assumed to be expressed by a trigonometric function, $\cos(\phi - \pi/4)$, for convenience of numerical calculations. Dephasing constant Γ^+_{ijkl} was calculated by using the FFT program package. The differential equations for diagonal and off-diagonal density matrix elements, eqs 10 and 12, with an initial condition were solved by using the fourth-order Runge−Kutta method. Here, the density matrix elements of $\rho(t)$ are represented as an 800 × 800 matrix to obtain converged results.

Figure 5 shows dephasing effects in the time-dependent expectation values of the rotational angular momentum $l(t)$ of the pentacene rotor. The upper panel shows the circularly polarized electric field components, $E_X(t)$ and $E_Y(t)$, applied to the rotor. It can be seen from Figure 5 that the instantaneous angular momentum of the rotor synchronously oscillates with the applied field just after the excitation. This originates from the fact that both the frequency of the applied field and that of the pendulum motion of the rotor are of the same order, and the adiabatic condition breaks down.

In Figure 5, $l(t)$ is evaluated for three different values of the system−bath coupling η. For $\eta = 0$, where there is no system−bath coupling, unidirectional rotation with positive values of $l(t)$ starts at about $t = 0.2$ ns after several cycles of pendulum motions, and at around $t = 0.3$ ns $l(t)$ reaches a constant unidirectional rotation with ca. 65 $\hbar$.

For $\eta = 0.01$, where dephasing time above potential barrier $\Delta U = 288$ cm^{-1} is estimated to be about 20 ps, a positive angular momentum with maximum $l(\tau_p) =$ ca. 40 $\hbar$ is created

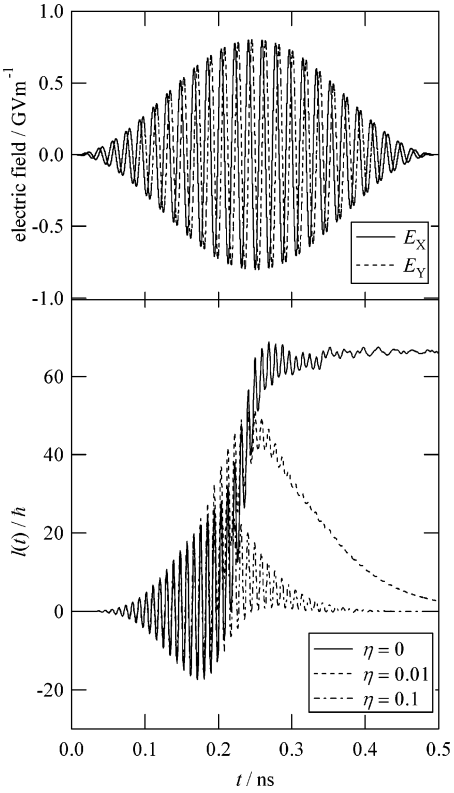

Figure 5. Top panel: X and Y components of circularly polarized electric field vector $\boldsymbol{E}(t)$ applied. Bottom panel: instantaneous angular momentum of the molecular rotor $l(t)$ with system-bath coupling η.

at around $t = 0.25$ ns when the electric field reaches the maximum but decays as the electric field fades out. It should be noted that $l(t)$ for $= 0$ takes lower value than that for $\eta = 0.01$ around $t = 0.2$ ns. That is, the averaged angular momentum in the absence of the system−bath coupling is temporally smaller than that in the presence of the coupling. This anomalous behavior was caused by the rapid rising of the electric field envelope in the early stage, and the behavior disappears by setting τ_p longer.

Under a further faster dissipative condition with $\eta = 0.1$, where dephasing time above the potential barrier is ca. 2 ps, an unstable unidirectional rotation is created around at $t = 0.25$−0.30 ns, in which the electric field has maximum intensity, and disappears before the electric field fades out. To continue rotation, it is necessary to apply an electric field with increasing intensity before the rotor reaches a local equilibrium condition.

4. Conclusion

A molecular rotor made of pure hydrocarbons is theoretically designed within the semiclassical treatment of the rotor−electric field interactions. Rotors with relatively high polarizabilities are driven by a circularly polarized electric field through induced-dipole interactions for nonresonant cases. Electric fields in a regime of mm wavelengths (GHz) are required to effectively drive such a rotor due to the large moment of inertia of the rotor. Related to this, a new spectroscopy using millimeter electric fields has recently been proposed in addition to THz spectroscopy.[30−32] A pentacene rotor was adopted for demonstration of rotations. Equations of motions for the density matrix derived within the Redfield treatment were numerically solved to investigate dephasing effects due to short-range interactions between the rotor of interest and heat bath substances. Rotors driven by electric fields reach a local equilibrium with the

Boltzmann distribution at a temperature higher than that in the heat bath and then stop rotational motions. The thermal energy in the local equilibrium is comparable to the internal rotation barrier ΔU.

Finally, actual motors are described in terms of rotation speed and torque. The rotation speed of the pentacene rotor is shown in Figure 5. The torque created by the pulsed electric field from $t = 125-375$ ps, for example, under condition of $\eta = 0$ can roughly be estimated as $65\ \hbar/250\ \text{ps} = 2.6 \times 10^{-23}$ Nm.

Acknowledgment. This work was supported in part by a Grant-in-Aid for Scientific Research from the Ministry of Education, Science, Sports, Culture and Technology, Japan (no. 17350004). F.P. thanks the COE program "Giant Molecules and Complex Systems" of Tohoku University for financial support. M.Y. acknowledges the receipt of a COE Fellowship (no. 12180010).

References and Notes

(1) Kay, E. R.; Leigh, D. A.; Zerbetto, F, *Angew. Chem., Int. Ed*. **2007**, *46*, 72−191.

(2) Kottas, G. S.; Clarke, L. I.; Horinek, D.; Michl, J. *Chem. Rev.* **2005**, *105*, 1281−1376.

(3) Kinbara, K.; Aida, T. *Chem. Rev.* **2005**, *105*, 1377−1400.

(4) *Molecular Machine and Motors*; Sauvage, J.-P., Ed.; Springer: Berlin, **2001**; Vol. 99, Structure and Bonding.

(5) Kelly, T. R.; Silva, R. A.; Silva, H. D.; Jasmin, S.; Zhao, Y. *J. Am. Chem. Soc*. **2000**, *122*, 6935−6949.

(6) Bedard, T. C.; Moore, J. S. *J. Am. Chem. Soc.* **1995**, *117*, 10662−10671.

(7) Balzani, V.; Gomez-Lopez, M.; Stoddart, J. F. *Acc. Chem. Res*. **1998**, *31*, 405−414.

(8) Tuzun, R. E.; Noid, D. W.; Sumpter, B. G. *Nanotechnology* **1995**, *6*, 52−63.

(9) Sauvage, J.-P. *Acc. Chem. Res.* **1998**, *31*, 611−619.

(10) Hess, H.; Bachand, G. D.; Vogel, V. *Chem.—Eur. J.* **2004**, *10*, 2110−2116.

(11) Easton, C. J.; Lincoln, S. F.; Barr, L.; Onagi, H. *Chem.—Eur. J.* **2004**, 3120−3128.

(12) (a) Vacek, J.; Michl, J. *New J. Chem*. **1997**, *21*, 1259−1268. (b) Vacek, J.; Michl, J. *Proc. Natl. Acad. Sci. U.S.A.* **2001**, *98*, 5481−5486. (c) Horinek, D.; Michl, J. *J. Am. Chem. Soc.* **2003**, *125*, 11900−11910.

(13) Wang, H.; Oster, G. *Appl. Phys. A* **2002**, *75*, 315−323.

(14) Mandl, C. P.; König, B. *Angew. Chem., Int. Ed.* **2004**, *43*, 1622−1624.

(15) Hawthorne, M. F.; Zink, J. I.; Skelton, J. M.; Bayer, M. J.; Lui, C.; Livshits, E.; Baer, R.; Neuhauser, D. *Science* **2004**, *303*, 1849−1851.

(16) (a) Koumura, N.; Zijlstra, R. W. J.; van Delden, R. A.; Harada, N.; Feringa, B. L. *Nature* **1999**, *401*, 152−155. (b) Feringa, B. L.; Koumura, N.; van Delden, R. A.; ter Wiel, M. K. J. *Appl. Phys. A* **2002**, *75*, 301−308. (c) van Delden, R. A.; ter Wiel, M. K. J.; de Jong, H.; Meetsma, A.; Feringa, B. L. *Org. Biomol. Chem.* **2004**, *2*, 1531−1541. (d) van Delden, R. A.; ter Wiel, M. K. J.; Pollard, M. M.; Vicario, J.; Koumura, N.; Feringa, B. L. *Nature* **2005**, *437*, 1337−1340.

(17) Bermudez, V.; Capron, N.; Gase, T.; Gatti, F. G.; Kajzar, F.; Leigh, D. A.; Zerbetto, F.; Zhang, S. *Nature* **2000**, *406*, 608−611.

(18) Wang, Q. C.; Qu, D. H.; Ren, J.; Chen, K.; Tian, H. *Angew. Chem., Int. Ed.* **2004**, *43*, 2661−2665.

(19) (a) Mobian, P.; Kern, J. M.; Sauvage, J. P. *Angew. Chem., Int. Ed.* **2004**, *43*, 2392−2395. (b) Collin, J. P.; Sauvage, J. P. *Chem. Lett.* **2005**, *34*, 742−747.

(20) (a) Hoki, K.; Sato, M.; Yamaki, M.; Sahnoun, R.; González, L.; Koseki, S.; Fujimura, Y. *J. Phys. Chem. B* **2004**, *108*, 4916−4921. (b) Hoki, K.; Yamaki, M.; Koseki, S.; Fujimura, Y. *J. Chem. Phys.* **2003**, *118*, 497−504. (c) Hoki, K.; Yamaki, M.; Fujimura, Y. *Angew. Chem., Int. Ed*. **2003**, *42*, 2975−2978. (d) Hoki, K.; Yamaki, M.; Koseki, S.; Fujimura, Y. *J. Chem. Phys.* **2003**, *119*, 12393−12398. (e) Yamaki, M.; Hoki, K.; Ohtsuki, Y.; Kono, H.; Fujimura, Y. *J. Am. Chem. Soc.* **2005**, *127*, 7300−7301. (f) Yamaki, M.; Hoki, K.; Ohtsuki, Y.; Kono, H.; Fujimura, Y. *Phys. Chem. Chem. Phys.* **2005**, *7*, 1900−1904.

(21) Fujimura, Y.; González, L.; Kröner, D.; Manz, J.; Mehdaoui, I.; Schmidt, B. *Chem. Phys. Lett.* **2004**, *386*, 248−253.

(22) Viala, C.; Secchi, A.; Gourdon, A. *Eur. J. Org. Chem.* **2002**, 4185−4189.

(23) Jian, H.; Tour, J. M. *J. Org. Chem*. **2003**, *68*, 5091−5103.

(24) Anthony, J E.; Eaton, D L.; Parkin, S. R. *Org. Lett.* **2002**, *4*, 15−18.

(25) Dion, C. M.; Keller, A.; Atabek, O.; Bandrauk, A. D. *Phys. Rev. A* **1999**, *59*, 1382−1391.

(26) Redfield, R. G. *IBM J. Res. Dev.* **1957**, *1*, 19−31.

(27) Blum, K. *Density Matrix Theory and Applications*; Plenum Press: New York, 1981.

(28) Pollard, W. T.; Felts, A. K.; Friesner, R. A. *Adv. Chem. Phys.* **1996**, *93*, 77−134.

(29) Becke, D. A. *J. Chem. Phys.* **1993**, *98*, 1372−1377.

(30) Beard, M. C.; Turner, G. M.; Schmuttenmaer, C. A. *J. Phys. Chem. B* **2002**, *106*, 7146−7159.

(31) Schmuttenmaer, C. A. *Chem. Rev*. **2004**, *104*, 1759−1779.

(32) Steeves, A. H.; Bechtel, H. A.; Coy, S. L.; Field, R. W. *J. Chem. Phys.* **2005**, *123*, 141102-1−141102-4.